JCTC Journal of Chemical Theory and Computation
Article
pubs.acs.org/JCTC

# Direct *ab Initio* (Meta-)Surface-Hopping Dynamics

David B. Lingerfelt, David B. Williams-Young, Alessio Petrone, and Xiaosong Li*

Department of Chemistry, University of Washington, Seattle, Washington 98195, United States

**ABSTRACT:** Tractable methods for studying the molecular dynamics of chemical processes driven by electronic nonadiabaticity are highly sought after to provide insight into, for example, photochemical reaction mechanisms, molecular collisions, and thermalized electronic band structures. Starting from the time-dependent Schrödinger equation for a many-body system, a direct *ab initio* trajectory surface-hopping (TSH) method relying on an analytical treatment of nonadiabatic couplings between electronic states is developed in this work. An approach that combines time-dependent perturbation theory and explicit time evolution via TSH to expedite calculation of nonadiabatic transition rates, namely, meta-surface-hopping dynamics, is presented, and an extrapolatory approach using time-dependent perturbation theory for recovering unbiased transition rates is assessed. The meta-surface-hopping method is applied to the problem of estimating nonradiative relaxation rates of a photoexcited iminium ion, $CH_2NH_2^+$, and evidence for internal consistency of the combined dynamics/perturbation theory approach is presented.

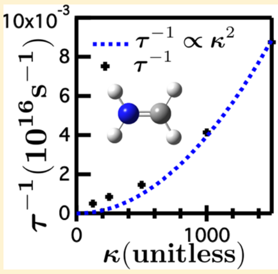

Time-dependent perturbation theory can properly account for effects of magnifying non-adiabatic coupling strength on non-radiative decay rates from surface hopping dynamics

## 1. INTRODUCTION

The prediction of molecular systems' time evolution from first principles provides a means to study fundamental chemical processes with spatial and temporal resolution unparalleled by most experiments.[1−3] Time-domain simulations of chemical systems can, for example, be used to reproduce absorption spectra with realistically broadened line shapes,[4−7] resolve mechanisms of complex chemical transformations,[8,9] and obtain rate constants for nonequilibrium processes.[10,11] The exact chemical dynamics (in the nonrelativistic limit at least) are well known to result from integration of the time-dependent Schrödinger equation (TDSE, eq 1).

$$i\dot{\Psi}(\mathbf{R}, \mathbf{r}; t) = \mathcal{H}(\mathbf{R}, \mathbf{r}; t)\Psi(\mathbf{R}, \mathbf{r}; t) \tag{1}$$

$\mathcal{H}$, the molecular Hamiltonian, is the generator of time translations for the molecular wave function $\Psi$, which depends explicitly on nuclear and electronic degrees of freedom (DOF) $\mathbf{R}$ and $\mathbf{r}$, and parametrically on time, $t$. The molecular Hamiltonian expressed in the atomic unit system (used throughout this report) is given in eq 2.

$$\begin{aligned}\mathcal{H} &= -\sum_a \frac{1}{2M_a}\nabla^2_{\mathbf{R}_a} - \sum_b \frac{1}{2}\nabla^2_{\mathbf{r}_b} + V(\mathbf{r}, \mathbf{R}) \\ &= -\sum_a \frac{1}{2M_a}\nabla^2_{\mathbf{R}_a} + \mathcal{H}_r(\mathbf{r}, \mathbf{R})\end{aligned} \tag{2}$$

Here, $a$ and $b$ index the nuclear and electronic DOF, respectively, $M_a$ is the mass of nuclei $a$, and $V(\mathbf{r}, \mathbf{R})$ is the total potential energy operator collecting all electrostatic interaction terms between electrons and nuclei. Eigenfunctions of the last two terms in eq 2 (i.e., the functions $\{\Phi_i\}$ which solve the time-*independent* electronic Schrödinger equation, $\mathcal{H}_r(\mathbf{r}, \mathbf{R})\Phi_i(\mathbf{r}; \mathbf{R}) = E_i(\mathbf{R})\Phi_i(\mathbf{r}; \mathbf{R})$), form a complete basis at each $\mathbf{R}$ in which $\Psi$ may be expanded. Similarly resolving the nuclear wave functions associated with each $\Phi_i$ in their energy eigenbasis requires *a priori* knowledge of global electronic potential energy surfaces (PESs), i.e., eigenvalues of $\mathcal{H}_r(\mathbf{r}, \mathbf{R})$ for all $\mathbf{R}$ where the nuclear wave function is nonvanishing.[12−14] Nonclassical nuclear phenomena such as tunneling and zero-point energy formally mandate treatment in terms of the quantized nuclear energy levels. For heavier nuclei at moderately high temperatures, these effects are negligible, and treating the nuclei classically and electrons quantum mechanically is only a mild approximation. These "mixed quantum—classical" (MQC) formalisms[15−17] offer a favorable compromise between accuracy and computational expense in this case, and the system can be selectively partitioned to allow a subset of nuclear DOF to be treated quantum mechanically.[11,18]

This simplest of the MQC methods neglects the exciton—phonon coupling altogether, under the assumption that electronic eigenstates are well separated relative to the nuclear kinetic energy (i.e., the Massey parameter <1).[19−21] When this assumption is not satisfied, electronically nonadiabatic evolution can dominate the dynamics, and the effect which slow particle motions exert on the fast particles evolution (and *vice versa*) must be included to recover the correct dynamics.

To account for the coupled PESs, the electronic wave function can be allowed to evolve into a superposition of eigenstates which mix according to the nondiagonality of the nuclear kinetic energy operator in the electronic energy eigenbasis. The enormous complication that results from relaxing the electronic adiabaticity constraint is that nuclear dynamics are no longer strictly amenable to classical treatment. Components of the superposition associated with excited electronic states would exhibit proportionately lower nuclear momenta, inevitably leading to delocalization of the nuclear

**Received:** July 22, 2015
**Published:** February 8, 2016

Downloaded via LAWRENCE BERKELEY NATL LABORATORY on August 17, 2018 at 16:56:12 (UTC).
See https://pubs.acs.org/sharingguidelines for options on how to legitimately share published articles.

ACS Publications © 2016 American Chemical Society

DOI: 10.1021/acs.jctc.5b00697
*J. Chem. Theory Comput.* 2016, 12, 935−945

wave function over time. One approximation to circumvent this dilemma is to let the nuclei experience the expectation value of the force evaluated for the electronic superposition. In this way, the nuclei experience the "mean field" forces of the vibrationally coupled electronic states, an approach often referred to as Ehrenfest dynamics. The nuclear delocalization problem is avoided at the cost of foregoing dynamical electron−nuclear correlations in this framework. This shortcoming causes a lack of microscopic reversibility and, therefore, detailed balance[22] that leads to spurious energy transfer from the slow to fast DOF.[23,24] Even still, short-time dynamics of systems exhibiting significant nonadiabatic coupling are often well approximated with the Ehrenfest approach, and detailed balance can be artificially restored somewhat through application of thermostats[18] or by externally reintroducing electron−nuclear dynamical correlation back into the propagated state.[25,26]

Multiconfigurational mixed quantum−classical approaches (e.g., Multiple Spawning,[27] Ring Polymer[28,29]/Centroid[30] MD, etc.) capture correlations in the fast and slow DOF but scale less favorably than the mean field method due to increased dimensionality of their molecular wave function *ansatz*. Reviews of the performance and expense of these multiconfigurational techniques are found elsewhere in the literature.[31−33] Independent trajectory surface-hopping (TSH) approaches have been introduced in an effort to decouple the evolution of nuclear wave functions associated with different electronic states[34,35] and often produce results that align favorably with experimental and full quantum dynamics.[36−38] Swarms of independent TSH trajectories offer a stochastic sampling of the dynamical electron−nuclear correlation neglected by the mean field dynamics. Since TSH permits deviation of the nuclear trajectories from the majority probability time-evolution channel, it is better suited for exploring dynamics initiated by rare events than the Ehrenfest scheme. These minority probability nuclear evolution channels are important to the dynamics of systems undergoing, e.g., photochemical processes and high-energy collisions.

While there are numerous implementations of TSH dynamics intended for use alongside electronic structure theory packages,[36,37,39−43] most of the previous works resort to making computationally affordable approximations for the excited state potential energy surfaces, treatment of the quantum "back-reaction" describing the effect that electronic transitions exert on the nuclear evolution, and/or evaluation of the nonadiabatic couplings. With the recent derivations of analytical derivative couplings for low-scaling, single-reference electronic structure formalisms[44−49] and ever-increasing computational power, it becomes possible to carry out first-principles, on-the-fly, surface-hopping dynamics.

In this report, a direct *ab initio* surface-hopping method is presented for studying nonradiative decay processes induced by electronic nonadiabaticity. Electronic energies, analytical forces, and nonadiabatic couplings are computed "on-the-fly". We also present an approach to expedite the acquisition of temporal properties of systems exhibiting nonadiabatic effects, relying on an external biasing procedure to accelerate the dynamics in a systematic, reproducible fashion. This approach will be referred to as the meta-surface-hopping method. The implementation outlined here uses the random phase approximation (RPA) with either a Hartree−Fock or density functional theory ground (reference) state to treat the many-body problem for excited electronic states,[50−61] accounting for the effect of electronic transitions on the nuclear dynamics and making use of analytical expressions for the nonadiabatic coupling between electronic states. Thus, our implementation is designed to capture all of the requisite physics to accurately predict electron−phonon scattering processes for general molecular and condensed-phase systems and also to be compatible with meta-surface-hopping.

We begin by presenting a brief overview of the necessary formalism to motivate the meta-surface-hopping method and then present working equations and pseudocode for the numerical integration of the molecular equations of motion along with the TSH algorithm. Finally, we introduce the meta-surface-hopping biasing scheme which combines the benefits of TSH and time-dependent perturbation theory to accelerate the evaluation of dynamical properties of electronically nonadiabatic systems. The developed concepts are then applied to a test case that expedites the calculation of nonradiative decay rates for a small photoexcited model system.

## 2. METHODOLOGY

**2.1. Review of Surface-Hopping Method.** To arrive at a method capable of capturing the dynamical correlations between electronic and nuclear DOF, a multiconfiguration *ansatz* for the molecular wave function is first posited:

$$\Psi(\mathbf{R}, \mathbf{r}, t) = \sum_k \Omega_k(\mathbf{R}, t)\Phi_k(\mathbf{r}, \mathbf{R}) \tag{3}$$

Here, we have associated a many-body nuclear wave function, $\Omega_k$, with each electronic adiabat, $\Phi_k$, where a complex exponential "phase factor" between the electronic and nuclear wave functions has been implicitly absorbed into each $\Omega_k$. Substituting this *ansatz* into eq 1, multiplying on the left by $\Phi_j^*(\mathbf{r}, \mathbf{R})$, and integrating over $\mathbf{r}$ yields the Schrödinger equation for the nuclear wave functions:

$$i\frac{\partial\Omega_k(\mathbf{R}, \mathbf{t})}{\partial t} = -\sum_a \frac{1}{2M_a}\nabla^2_{\mathbf{R}_a}\Omega_k(\mathbf{R}, t) + E_k(\mathbf{R})\Omega_k(\mathbf{R}, t) + \sum_{a,j}\left(\frac{1}{2M_a}D^a_{kj}\Omega_j(\mathbf{R}, t) - \frac{1}{M_a}d^a_{kj}\cdot\frac{\partial\Omega_j(\mathbf{R}, t)}{\partial\mathbf{R}_a}\right) \tag{4}$$

where we have made the following definitions:

$$d^a_{kj} = \langle\Phi_k|\partial\Phi_j/\partial\mathbf{R}_a\rangle \tag{5}$$

$$D^a_{kj} = \langle\Phi_k|\partial^2\Phi_j/\partial\mathbf{R}_a^2\rangle \tag{6}$$

From eq 4, a physical picture for the nuclear evolution emerges. Piecewise application of Ehrenfest's theorem to the first two terms in eq 4 gives the centers of the $k^{\text{th}}$ nuclear wave function evolving according to the curvature of the corresponding adiabatic PES. The third term contains the non-Hermitian second derivative couplings, $D_{kj}$, which contribute small corrections to the adiabatic nuclear kinetic energies and interstate couplings that are generally safe to neglect in this context.[62] The final term in eq 4 is primarily responsible for the mixing of the nuclear wave functions brought about by the nuclear momentum operator evaluated between adiabats, $d_{kj}$, which we aim to account for probabilistically with the TSH algorithm.

Since the goal is to arrive at a classical trajectory-based method, we promptly take the classical limit for the nuclear DOF by identifying each nuclear wave function with a

(Hartree) product of Dirac delta functions, $\delta(\mathbf{R} - \mathbf{R}_k(t))$, centered on the nuclei:

$$\Omega_i(\mathbf{R}, \mathbf{R}_k(t)) = c_k(t)\delta(\mathbf{R} - \mathbf{R}_k(t)) \tag{7}$$

The complex coefficients $\{c_k(t)\}$ collect the weights and phases for each product $(\Omega_k{\cdot}\Phi_k)$ contributing to the superposition state, and $\mathbf{R}_k(t)$ gives the coordinates of the classical nuclei evolving according to the forces from the $k^{\text{th}}$ adiabatic state. Note that $\langle\Phi_k|\dot{\Phi}_j\rangle = \dot{\mathbf{R}}_j(t)\cdot\langle\Phi_k|\nabla_{\mathbf{R}_j}|\Phi_j\rangle$ in the absence of any external time-dependent potential. Substituting the "classical nuclei" wave function *ansatz* for $\Omega$ (eq 7) back into the TDSE (eq 1) gives, with some straightforward algebraic manipulations, the equation of motion for $c_k(t)$:

$$\begin{aligned} i\dot{c}_k(t) &= \sum_j \underbrace{(\delta_{kj}\mathbf{V}_{jj} - i\dot{\mathbf{R}}_j(t)\cdot\mathbf{d}_{kj})}_{\mathbf{H}_{kj}} c_j(t) \\ &= \sum_j \mathbf{H}_{kj}c_j(t) \end{aligned} \tag{8}$$

where $\mathbf{V}_{\text{kj}} = \langle\Phi_k|\mathcal{H}_r|\Phi_j\rangle$. Since we choose to work in the adiabatic basis, $\{\Phi_j\}$ is the set of eigenfunctions of the electronic Hamiltonian and $\mathbf{V}$ becomes diagonal. Ehrenfest's theorem gives the time-dependence for the nuclear position and momentum expectation values equivalent to the Newtonian equation of motion (eq 9).

$$-\frac{\partial\mathbf{V}_{jj}}{\partial\mathbf{R}_j} = \mathbf{m}\ddot{\mathbf{R}}_{\mathbf{j}} \tag{9}$$

So, by taking the classical limit for the nuclear wave function associated with each electronic adiabat in the multiconfiguration wave function, we have arrived at a trajectory based method *of sorts*, where the nonadiabatic coupling between electronic energy eigenstates mixes the "classical" trajectories. Admitting the possibility of electronic transitions folds some uncertainty back into the nuclear positions, and the equations of motion we arrive at describe a delocalized superposition of otherwise sharply localized nuclei. The centers of the nuclear wave functions, $\{\mathbf{R}_k\}$, spread according to the disparate forces they encounter along their respective electronic PESs. As a result, even if the system is initially prepared in an eigenstate of the nuclear position operator, it may not remain so as the nuclei move. Instead, $c_k(t)c_k(t)^*$ gives the probability of observing the system in the $k^{\text{th}}$ nuclear position eigenstate at time $t$. More generally, $\rho_{jk}(t) = c_j(t)c_k^*(t)$ are elements of the one-particle reduced density matrix.[63] The notion of classical nuclei acting as observers of the quantum electronic state as they evolve has been explored in some recent non-TSH developments in the field of nonadiabatic dynamics.[64]

The state of the system is propagated by integrating the coupled set of differential eqs (eqs 8 and 9). However, as the $\mathbf{R}_k$ terms in eq 8 begin to delocalize, the matrix elements $\mathbf{d}_{jk}$ also become nonlocal, sharply increasing the cost of evaluating the dynamics.[65,66] For the sake of practicality, an "independent trajectory approximation" is invoked in which nuclear evolution on each electronic energy eigenstate is assumed identical, i.e., $\mathbf{R}_k(t) = \mathbf{R}_0(t)$ for all $k$. Electron−nuclear coherence is spuriously enforced in each trajectory under this approximation, and error is accrued in $\{c_k(t)\}$ since nuclear wave functions evolving on the different PESs should dephase from one another, diminishing (on average) their overlap.[67,68] The $\{c_k(t)\}$ from a given independent trajectory no longer individually represents the temporal behavior of the system. However, error in the independent trajectories' $\{c_k(t)\}$ can be partially removed by taking the population-weighted average of the $\{c_k(t)\}$ over all possible trajectories (started from the same initial conditions) that would result from at each instant in time allowing the nuclei to evolve according to the forces of each adiabat.[69] It is easy to show that number of these speculative trajectories increases *factorially* in time. However, the most heavily weighted trajectories in the average can be preferentially sampled so that error in $\{c_k(t)\}$ can be minimized with subfactorial time complexity.

From this notion sprung the TSH algorithm. Nuclei evolve according to the curvature of a single adiabatic state's PES, with stochastic switches of the state that contribute the instantaneous forces ("surface-hoping") during each TSH trajectory.[35] At a given time, the probability of the system being observed in nuclear position eigenstate $k$ (given by $|c_k(t)|^2$) determines the probability of the $k^{\text{th}}$ state contributing the nuclear forces. In this way, a set (or "swarm") of TSH trajectories recovers the branching statistics of bifurcating nuclear trajectories to account for the dynamic correlation between $\{c_k(t)\}$ and nuclear forces in each trajectory, while simultaneously ensuring that the average behavior of the nuclear dynamics across many trajectories is consistent with the average $\{c_k(t)\}$.

The probability of switching the state from $k$ to $j$, which minimizes the number of switches[11,70] required to maintain average nuclear forces consistent with $\{c_k(t)\}$ across a swarm of trajectories, is given by

$$g_{jk}(t + \Delta t_n) = \int_t^{t+\Delta t_n} dt' \frac{-2\mathbb{R}\text{e}(c_k(t')c_j^*(t'))\dot{\mathbf{R}}_0(t')\cdot\mathbf{d}_{kj}(t')}{c_j(t')c_j^*(t')} \tag{10}$$

$g_{jk}(t)$ is compared to a uniformly distributed random number, $\eta$, on the open interval (0,1). If $g_{jk} \leq \eta$, no hop occurs, and the numerical integration of eqs 8 and 9 continues with no change in the state contributing the nuclear forces. If $g_{jk} > \eta$, then the component of the nuclear momentum along $d_{jk}$ is checked to ensure the nuclear kinetic energy along the coupling vector is greater than or equal to the difference in potential energy of the two states. If so, the hop is accepted, nuclear momenta are rescaled to conserve total energy, and the forces that dictate the evolution of the nuclei in the next time step will be those of state $k$. Otherwise, the hop is rejected. Because classically forbidden hops are disallowed, the TSH approximately satisfies detailed balance and reproduces the Boltzmann distribution for electronic state populations at long times.[23] This strict energy conservation condition can also be relaxed somewhat according to the time−energy uncertainty relation to account for nuclear tunneling events that manifest as classically forbidden transitions.[71]

### 2.2. Direct *Ab Initio* Surface-Hopping Algorithm Using a Split Integrator.

Since the characteristic time scales on which the electronic and nuclear DOF evolve differ by many orders of magnitude, split time-scale integration schemes can be safely applied to promote computational efficiency. In the following section, we describe our implementation of the direct *ab initio* fewest switches TSH method in the development version of the Gaussian[72] suite of electronic structure programs with interface to the direct BOMD algorithm.[73,74] In the direct formalism, all components of the TSH method, including the

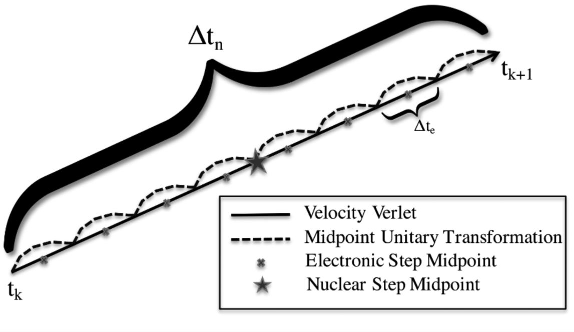

```
for $1 \le k \le maxstep$ do
    Get $\mathbf{V}(t_k)$ for all states
    Get $\mathbf{d}(t_k)$ between all states
    Get $\nabla_{R_0}\mathbf{V}(t_k)$ for current state
    if (not first step since start/hop) then
        Propagate $\dot{\mathbf{R}}_\mathbf{0}(t_{k-1/2}) \to \dot{\mathbf{R}}_\mathbf{0}(t_k)$ (Eq. (11a))
        for $1 \le j \le (\Delta t_n/\Delta t_e)$ do
            Use $\mathbf{U}(t_{j+1/2})$ to Propagate $\mathbf{c}(t_j) \to \mathbf{c}(t_{j+1})$ (Eqs. (14) to (16))
            Calculate (and collect) integrand of Eq. (10) scaled by $\Delta t_e$
        end for
        Compare each $g$ to uniformly distributed random number $\eta \in \mathcal{U}\{0,1\}$
        if $g > \eta$ then
            Calculate kinetic energy component along coupling vector, $T_d$
            if $T_d > \Delta\mathbf{V}$ then
                Switch current state
                Scale $\dot{\mathbf{R}}_\mathbf{0}$ to conserve total energy
            end if
        else
            Calculate $\mathbf{R}_\mathbf{0}(t_{k+1})$ and $\dot{\mathbf{R}}_\mathbf{0}(t_{k+1/2})$ (Eqs. (11b) to (11c))
        end if
    end if
end for
```

**Figure 1.** Schematic representation of the split time-scale integration scheme used in the current implementation.

potential energy, force, and nonadiabatic coupling are computed “on-the-fly”.

In the current work, eq 9 is integrated numerically by the velocity Verlet algorithm:

$$\dot{\mathbf{R}}_0\left(t + \frac{1}{2}\Delta t_n\right) = \dot{\mathbf{R}}_0(t) + \frac{1}{2}\ddot{\mathbf{R}}_0(t)\Delta t_n \tag{11a}$$

$$\mathbf{R}_0(t + \Delta t_n) = \mathbf{R}_0(t) + \dot{\mathbf{R}}_0\left(t + \frac{1}{2}\Delta t_n\right) \tag{11b}$$

$$\dot{\mathbf{R}}_0(t + \Delta t_n) = \dot{\mathbf{R}}_0\left(t + \frac{1}{2}\Delta t_n\right) + \frac{1}{2}\ddot{\mathbf{R}}_0(t + \Delta t_n)\Delta t_n \tag{11c}$$

with nuclear time step $\Delta t_n$.

Equation 8 can equivalently be expressed in matrix/vector notation (eq 12).

$$i\dot{\mathbf{c}}(t) = \mathbf{H}(t)\mathbf{c}(t) \tag{12}$$

The vector of complex coefficients, $\mathbf{c}(t)$, is propagated here using a midpoint unitary transformation method:[75,76]

$$\mathbf{c}(t + \Delta t_e) = \mathbf{U}\left(t + \frac{1}{2}\Delta t_e\right)\mathbf{c}(t) \tag{13}$$

$$\mathbf{U}(t) = \exp[-i\mathbf{H}(t)\Delta t_e] \tag{14}$$

where $\Delta t_e$ is the electronic time step. The matrix exponentiation is carried out by first expressing $\mathbf{H}(t)$ in its eigenbasis:

$$\mathbf{H}(t) = \mathbf{\Lambda}(t)\boldsymbol{\epsilon}(t)\mathbf{\Lambda}^\dagger(t) \tag{15}$$

Then the propagator can be easily constructed:

$$\mathbf{U}(t) = \mathbf{\Lambda}(t)\exp[-i\Delta t_e\boldsymbol{\epsilon}(t)]\mathbf{\Lambda}^\dagger(t) \tag{16}$$

The hopping probabilities defined in eq 10 are conveniently evaluated by numerical integration with the same discrete time step utilized in the electronic propagation. At each step in the numerical integration of eq 8, the integrand of eq 10 is evaluated and multiplied by the electronic time step. These values are summed over the course of the nuclear step to give the left Riemann sum approximation to the integral in eq 10. Analytical expressions for the nonadiabatic couplings for states represented in the electronic structure framework of RPA or linear response TDDFT have been previously derived by numerous groups.[44−49] A slightly different derivation of the working equations used in this work to calculate first-order nonadiabatic coupling matrix elements between the ground and excited states resolved via random phase approximation (RPA, i.e., “linear response TDDFT/TDHF”) based methods is given in the Appendix 1.

Since the nuclei at all times evolve according to the forces associated with a single adiabatic state (and nuclear momenta are explicitly rescaled after hops to conserve total energy), energy conservation of exactly the same quality as the adiabatic "Born-Oppenheimer" molecular dynamics (BOMD) is trivially guaranteed by the surface-hopping algorithm. Both the velocity Verlet and midpoint methods are second-order integration schemes. However, since the $\mathbf{d}_{jk}$, $\dot{\mathbf{R}}_0$, and $\mathbf{V}_{jj}$ are calculated only at intervals of $\Delta t_n$, these quantities are interpolated between $t$ and $t + \Delta t_n$ to account for their linear changes during nuclear time steps in the electronic propagation (see Figure 1 for schematic representation and pseudocode.) This interpolation complicates the error analysis of the resulting method somewhat since it is a source of error in the electronic propagation that is not a result of the inaccuracy of the numerical integration of eq 12 but of the assumed linearity of the interpolated quantities across the nuclear time step. The nuclear time step should therefore be chosen sufficiently small to not only conserve total energy of the system as in the BOMD scheme but also to not under-sample regions of the nuclear phase space where $\mathbf{d}$ is nonlinear in $\mathbf{R}$ over the distance $\dot{\mathbf{R}}\cdot\Delta t_N$.

When the nuclear evolution brings two adiabats into degeneracy, the derivative couplings ($\mathbf{D}$ and $\mathbf{d}$) between those states become unboundedly large in magnitude and the involved PESs exhibit discontinuities. When these regions of strong coupling are extremely localized in the nuclear phase space, the finite time-step of the nuclear dynamics can cause the crossing points to be skipped over in some trajectories. This scenario becomes more common for larger systems of weakly interacting fragments. In this case, it is common practice to utilize a basis of diabatic states since off-diagonal matrix elements of the electronic Hamiltonian in the diabatic representation are well defined even at PES crossings, and moreover these electronic couplings are generally well-behaved functions of the nuclear coordinates, $\mathbf{R}$.[77] Beyond transformation to a (locally quasi-)diabatic basis, approaches to identify PES crossings directly within the adiabatic basis based on the overlap of the electronic eigenfunctions at adjacent $\Delta t_N$ can also be utilized to enforce transition at PES crossings externally to the FSSH algorithm.[78,79]

### 2.3. Meta-Surface-Hopping Dynamics.

A longstanding criticism of TSH approaches has been the sheer quantity of trajectories that must be computed in order to ensure the convergence of results. If the dynamical process of interest occurs over long (∼*ns* and slower) time-scales, or is fast but initiated by some rare event, TSH is of little practical utility. In this section, we introduce a "meta-surface-hopping dynamics" method (MSH) for expediting the estimation of nonadiabatic relaxation time constants. This approach, in the similar spirit as the "meta-dynamics",[80,81] combines time-dependent perturbation theory (TDPT) with direct *ab initio* TSH to achieve an optimal balance of computational expense and accuracy. The central idea of the meta-dynamics approach is to bias the evolution of a system toward a desired low-probability pathway and then mathematically relate results of the biased dynamics to those for the unbiased system.[80,81] In this way, rare events can be efficiently investigated directly in the time domain, and the effect of the biasing on the resulting dynamics can be accounted for *post facto*. While the MSH method is certainly not the first method to be put forth for expediting the description of slow nonadiabatic processes in TSH,[82−84] the current work (to the authors' best knowledge) represents the first such attempt to combine the benefits of direct dynamics and TDPT to this end.

The choice of rare event biasing depends on whether or not there exists a mathematical expression that can resolve the effect of the biasing on the dynamical observables. TDPT is a reliable method, with some degree of scrutiny, for describing the response of a system in the instants following the application of a small perturbation. Recall that the rate of transition from state $i$ to $j$ mediated by a time-independent external potential can be approximated by the Fermi's golden rule (in atomic units) derived using TDPT:[85−87]

$$\Gamma_{ij} = 2\pi|\langle\Phi_i|\dot{\Phi}_j\rangle|^2\delta(E_i - E_j) \tag{17}$$

A quasi-static approximation may be used to cast eq 17 into a time-dependent expression:

$$\Gamma_{ij}(t) = 2\pi|\langle\Phi_i(t)|\dot{\Phi}_j(t)\rangle|^2\delta(E_i(t) - E_j(t)) \tag{18}$$

As the character of the initial and final states change with nuclear motion, so does the transition rate. By following the explicit time evolution of the adiabats with molecular dynamics, the electronic states to which the Fermi's golden rule rate expression is applied are sampled from an ensemble of thermally accessible nuclear configurations. The ensemble-averaged expression for the transition rate is then given by

$$\langle\Gamma_{ij}\rangle = \frac{2\pi}{t'}\int_0^{t'} dt|\langle\Phi_i(t)|\dot{\Phi}_j(t)\rangle|^2\delta(E_i(t) - E_j(t)) \tag{19}$$

Using the chain rule, we can obtain the relationship between the nonadiabatic transition rate and the nonadiabatic coupling strength,

$$\begin{aligned}\langle\Gamma_{ij}\rangle &= \frac{2\pi}{t'}\int_0^{t'} dt|\dot{\mathbf{R}}_j(t)\cdot\langle\Phi_i|\nabla_{\mathbf{R}_j}|\Phi_j\rangle|^2\delta(E_i - E_j)\\ &= \frac{2\pi}{t'}\int_0^{t'} dt|\dot{\mathbf{R}}_j(t)\cdot\mathbf{d}_{ij}(t)|^2\delta(E_i - E_j)\end{aligned} \tag{20}$$

Equation 20 suggests that the time averaged nonadiabatic transition rate depends linearly on the nuclear kinetic energy ($\propto \dot{\mathbf{R}}^2$) and quadratically on the nonadiabatic coupling strength. Increasing the simulation temperature will increase the nonadiabatic transition rate. However, the nature of the dynamics will be severely modified as the nuclei are free to traverse different reaction pathways at substantially elevated temperatures. In contrast, there are two advantages of directly biasing the time-dependent nonadiabatic coupling in eq 20. First, it is a "cold" biasing technique in which the system temperature is not modified. Second, because of the quadratic dependence, one can quickly obtain a meaningful result without enforcing a large biasing.

In this work, we simply use and test a uniform biasing approach,

$$\mathbf{d}^{\text{biased}}(t) = \kappa\mathbf{d}(t) \tag{21}$$

where $\kappa$ is a time-independent biasing factor for all states and at all nuclear configurations. With such a biased time-dependent nonadiabatic coupling, it is rather easy to show from eq 20 that

$$\langle\Gamma^{\text{biased}}\rangle \approx \kappa^2\langle\Gamma^{\text{unbiased}}\rangle \tag{22}$$

With eq 22, the effect of biased time-dependent nonadiabatic coupling can be accounted for retroactively via first-order TDPT (i.e., Fermi's golden rule). Once well-converged results for the biased dynamics have been collected, one can relate the dynamics of the biased system back to those of the unbiased system via TDPT.

It is obvious that the dynamics are unaffected by the biasing in the limit of zero coupling, and the correct asymptotic behavior is ensured. Nonetheless, one must ensure that $\kappa$ is not so large that regions of the nuclear phase space that would be extensively sampled during the unbiased dynamics go unexplored as a result of overpromoted state switches. The stochastic nature of the surface-hopping algorithm builds in some insurance against this behavior, but in the event that excessive bias is applied, the dynamical processes that were rare in the unbiased dynamics dominate in the biased dynamics, and *vice versa*. Numerous trajectories would then be required to explore the regions of phase space that were frequently sampled in the unbiased dynamics, negating the practical advantage of applying the bias in the first place. Therefore, a balance must be struck in which the scaling factor is sufficiently large to promote the rare event but not so large as to preclude electronically adiabatic evolution in coupled regions of the adiabatic PES.

In general, one should seek to use the smallest $\kappa$ that produces nonadiabatic transitions at a rate that permits their study. The reaction coordinate for the nonadiabatic process can be characterized, and an appropriate range of scaling factors can be deduced from sample trajectories by analyzing the extent of sampling of the nuclear phase space prior to the nonadiabatic transition. Note that situations may arise in which the magnitudes of $\kappa$ needed to enable nonadiabatic processes to occur at a tractable rate do not uphold the "linear-response" regime in which the first-order TDPT is reliable. Not all unbiased observables are straightforwardly recoverable from the biased dynamics either. If a reliable relationship between the property of interest and the strength of the perturbation can be established (as is done here for the nonradiative transition rates by application of the Fermi's golden rule), the unbiased property can in principle be recovered from sufficiently many biased trajectories. However, the nuclear dynamics following a premature/late state switch relative to the unbiased dynamics can be substantially altered by the excess/deficit of energy transferred into nuclear momentum along the coupling vector when a hop occurs early/late relative to the unbiased rate. Observables that depend on a faithful reproduction of the nuclear dynamics following the nonadiabatic transition may therefore suffer substantial statistical degradation.

## 3. RESULTS AND DISCUSSION

In this work, we will demonstrate that nonadiabatic transition rates from the direct MSH dynamics are consistent with eq 22 derived from the TDPT expression. Details of a study validating the MSH approach on a single avoided crossing model problem are found in Appendix 2. As a practical test of the implementation outlined in the Methodology section, we performed a set of direct TSH trajectories to track the nonradiative decay of the first excited (singlet) state of protonated formaldimine, $H_2C{=}NH_2^+$. We simulate a Boltzmann ensemble of formaldimine molecules at room temperature (298 K). For a specific vibrational mode with a given Boltzmann sampled vibrational energy, the initial phase (nuclear positions and momenta) was chosen randomly and classically within the harmonic oscillator approximation.[88,89] The total angular momentum was set to zero. Since the real potential energy surface is not strictly harmonic, the initial vibrational coordinates and momenta generated by this procedure were scaled to correct for the anharmonicity. This ensemble assumes a broad geometric distribution of vibrational phases of the initial ground state from which the vertical excitation to the first singlet excited state takes place. A total of 40 initial conditions were prepared for dynamic studies. The electronic wave function was initialized as a pure state comprised exclusively of the first excited (singlet) state of the molecule in order to emulate a Franck−Condon type vertical photoexcitation of the molecule at time zero of the simulation. Five sets of trajectories from the 40 initial conditions were integrated for 1 ps, each employing a different biasing factor, $\kappa$, listed in Table 1. To enable direct comparison of results across the different sets of trajectories, identical initial conditions and random number generator seeds were used for the five different swarms. The values of $\Delta t_n$ and $\Delta t_e$ used in all simulations were 0.1 *fs* and 0.004 *fs*, respectively. These step sizes ensured energy conservation to within 0.03 kcal throughout the picosecond trajectories. In the following simulations, electronic degrees of freedom are modeled at the TDA-RPA-HF/6-31g(d,p) level of theory. Since the lower-scaling Tamm−Dancoff approximation (TDA) to the RPA yields nearly equivalent nonadiabatic couplings and excitation energies for the current system, TDA-RPA was used to resolve the excited state electronic structure in this case study.

**Table 1. Parameters for Nonradiative Decay Profile of $S_1$ State of $H_2C{=}NH_2^+$ Fit to a Function of the Form[a]: $f(t) = \mathrm{B}e^{-t/\tau_e} + (1 - B)e^{-t^2/2\tau_g^2}$**

| $\kappa$ | $\tau_e$ | $\tau_g$ | $B$ | $\tau$ | $\sigma^2$ |
|---|---|---|---|---|---|
| 125 | 745 | 2813 | 0.408 | 1970 | 0.055 |
| 250 | 3089 | 826 | 0.159 | 1185 | 0.033 |
| 500 | 673 | 717 | 0.841 | 680 | 0.028 |
| 1000 | 395 | 144 | 0.387 | 241 | 0.021 |
| 1500 | N/A | 114 | 0.0 | 114 | 0.022 |

[a] $\tau$ values are reported in units of $\Delta t_N$ or $s \times 10^{-16}$. $\sigma^2$ are the variances in the residuals for the fitted decay functions, calculated by the following: $\sigma^2 = \frac{1}{N-1}\sum_{i=1}^{N}(f(t_N)_{\mathrm{fit}} - f(t_N))^2$

Figure 2 shows the potential energy surfaces of the ground $S_0$ and the first excited state $S_1$ and the analytical nonadiabatic coupling strength as a function of C═N bond rotation of the

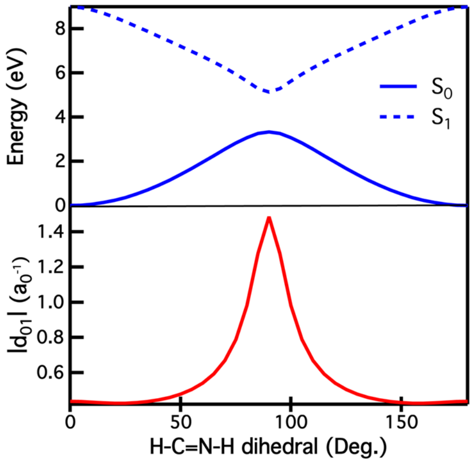

**Figure 2.** $S_0$ and $S_1$ PESs (top panel) and corresponding derivative coupling magnitude (bottom panel) as a function of H−C═N−H dihedral. All other internal coordinates are fixed at their equilibrium geometry values.

$H_2C{=}NH_2^+$ molecule. As expected, the energy gap between $S_0$ and $S_1$ states is the smallest when the C=N bond is rotated by 90° from the ground state equilibrium geometry, where the nonadiabatic coupling strength also reaches its maximum. However, the smallest gap is still ~1.8 eV, and the nonadiabatic coupling strength is only ~3 times larger than at the ground state equilibrium structure. This cursory analysis suggests that nonadiabatic transitions along this coordinate are rare events—an ideal test case to showcase the MSH dynamics.

As a benchmark for the effects of the biasing strategy on the PES sampling, we have plotted the density of nuclear position eigenstates (Figure 3) sampled prior to relaxation from $S_1$. At the largest $\kappa$ employed in this work, under-sampling of regions of the phase space occurs as a result of overpromotion of nonadiabatic transitions. The $\kappa = 1500$ dynamics would, in general, be discarded on these grounds, but the symmetry of the nuclear phase space for the particular system under investigation here makes the effect of the induced non-ergodicity less pronounced.

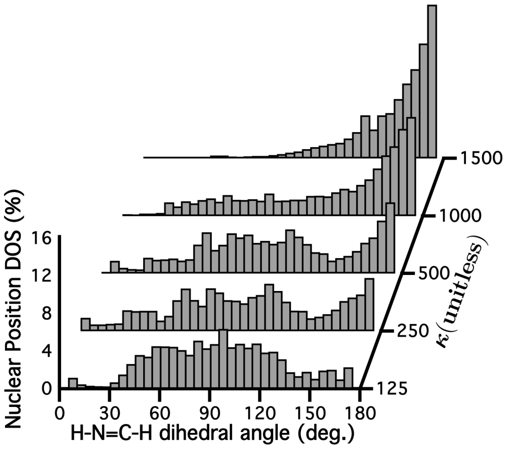

**Figure 3.** Histograms showing the density of nuclear position states sampled prior to relaxation to the ground state as a function of the biasing factor, $\kappa$. So as not to distinguish between the degenerate clockwise and counterclockwise rotation pathways about the double-bond in this analysis, identical configurations with respect to this symmetry have been binned together. Dihedrals are computed between the two hydrogens "*trans*" to one another in the initial condition, so that the "*cis*" and "*trans*" isomers are well defined and spurious nonergodic behavior in the DOS induced by large $\kappa$ can be resolved.

The decay profiles were fitted to Gaussian plus exponential functions (Figure 4). Since only two states are involved in the relaxation, multiexponential character is not expected in the decay profile. However, Gaussian-shaped relaxation profiles are included in the fitting function in order to quantify the non-Markovian, phonon memory-dependent contributions to the relaxation dynamics.[90] The resulting fit parameters and time constants for the decay are presented in Table 1, along with the explicit form of the fitting function, and plotted in Figure 5, along with the trendline of the form anticipated by the TDPT.

The resulting relaxation rates agree with the quadratic scaling predicted via the TDPT. Some of the deviation from the expected scaling can be attributed to the limited number of trajectories included in this investigation. Better agreement is seen for larger $\kappa$ where a greater portion of trajectories undergo hops. So, even though the same initial conditions were used for each swarm, the resulting rates are better statistically converged for the larger $\kappa$ cases (see variances of the residuals for each fitted function in Table 1)—another unique advantage for the MSH method. Once the required statistical convergence has been achieved for the relaxation rate at a few different biasing strengths, the decay constants can be fitted to a function that is quadratic in $\kappa$. The prefactor of the fitted quadratic function (Figure 5), $3.96 \times 10^7 s^{-1}$ for the current study, gives the MSH extrapolatory estimate for the relaxation rate for the unbiased system, i.e., for $\kappa = 1$. The results indicate that the studied process is indeed expected to be quite slow with respect to the time-step of the dynamics.

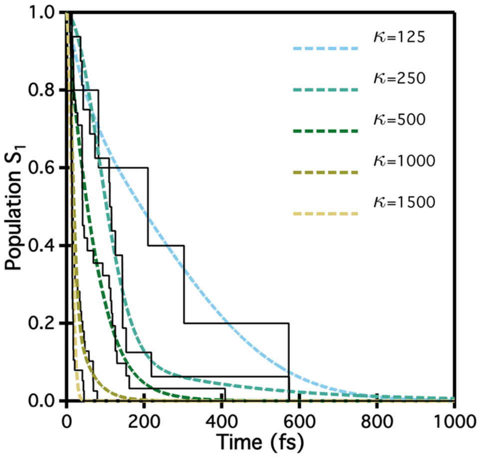

**Figure 4.** Examples of a vibrationally induced relaxation profile from $S_1$ state for $H_2C{=}NH_2^+$ resulting from the MSH dynamics with $\kappa$ = 125, 250, 500, 100, and 1500 (black traces) and corresponding exponential plus Gaussian fitted functions (colored, dashed traces).

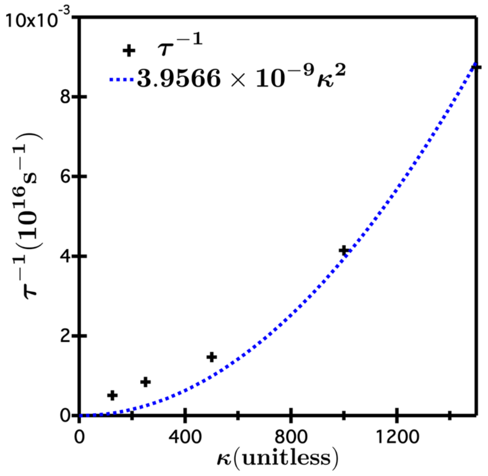

**Figure 5.** Plot of relaxation rates from Table 1 showing the trend for the relaxation rate ($\tau^{-1}$, black markers) as a function of the biasing factor, along with a least-squares fit of the rates as a function of biasing factor that is consistent with Fermi's golden rule (i.e., $\tau^{-1} \propto \kappa^2$).

## 4. CONCLUSION

In this report, we presented a direct *ab initio* (meta-)surface-hopping dynamics approach, where energies, analytical forces, and nonadiabatic couplings are computed "on-the-fly". A split integrator was implemented to facilitate the computation without compromising energy conservation. Analytical derivative coupling within the random phase approximation framework was derived and the working equations efficiently implemented. We also presented a time-dependent perturbation theory (TDPT)-based meta-dynamics approach to bias the dynamics toward nonadiabatic rare events. This approach aims to accelerate the acquisition of temporal properties of systems exhibiting electronic nonadiabaticity in a systematic, reproducible fashion.

As a test of the nonadiabatic meta-surface-hopping method, we calculated several sets of 40 trajectories with different biasing strengths for photoisomerizing protonated formaldimine. We have shown that the trend predicted via the TDPT expression holds when comparing the dynamics of swarms with different biasing factors, suggesting the internal consistency of our meta-dynamics/TDPT approach.

## ■ APPENDIX 1: FIRST-ORDER NONADIABATIC COUPLING MATRIX ELEMENTS BETWEEN GROUND AND EXCITED STATES

The mathematical expressions for derivative coupling within the random phase approximation (RPA) or the linear response TDDFT framework have have been previously presented by other groups.[44−49] Here, we present slightly different derivations for obtaining an efficient working expressions implemented in this work for the ground to excited state derivative coupling. In the present work, we adopt the notation that indices $i$, $j$, $k$, and $l$ refer to occupied molecular orbitals (MO); $a$, $b$, $c$, and $d$ refer to virtual MOs; and $p$, $q$, $r$, and $s$ refer to general MOs. The terms $\mu$, $\nu$, $\lambda$, and $\delta$ will be used to label atomic orbital (AO), and $\sigma$, $\sigma'$ terms label different spin orientations.

We cast the derivative coupling into second quantized form as a scattering problem off of a single body, anti-Hermitian operator, $\nabla_\xi$,

$$\nabla_\xi = \sum_{pq\sigma} \langle p;\, \sigma|\nabla_\xi|q;\, \sigma\rangle a^\dagger_{p\sigma} a_{q\sigma} \tag{A1}$$

where $a_p^\dagger$ and $a_q$ are the second quantized Fermionic creation and annihilation operators, respectively.

Recalling the expression for the nonadiabatic coupling (derivative coupling) with respect to nuclear coordinate $\xi$ between ground and $I$th excited state, $d^\xi_{0I}$, we may recast it into a general second quantized expression,

$$d^\xi_{0I} = \langle\Psi_0|\nabla_\xi|\Psi_I\rangle = \sum_{pq\sigma} \langle\Psi_0|a^\dagger_{p\sigma} a_{q\sigma}|\Psi_I\rangle\langle p;\, \sigma|\nabla_\xi|q;\, \sigma\rangle \tag{A2}$$

In the case where the ground state is expressed as a single Slater determinant of Hartree−Fock (HF) or Kohn−Sham (KS) orbitals, the $I$th excited state can be written as a non-Hermitian excitation operator $\hat{T}^I$ acting on the ground (reference) state,

$$|\Psi^I\rangle = \hat{T}^I|\Psi_0\rangle = \sum_{rs\sigma} t^I_{rs\sigma} a^\dagger_{r\sigma} a_{s\sigma}|\Psi_0\rangle \tag{A3}$$

For RPA and the Tamm−Dancoff approximation (TDA) thereof, the expression for $\mathbf{T}$ takes the convenient forms

$$\mathbf{T}^I_{\text{TDA}} = \begin{pmatrix} \mathbf{0} & \mathbf{0} \\ \mathbf{X}_I & \mathbf{0} \end{pmatrix} \quad \mathbf{T}^I_{\text{RPA}} = \begin{pmatrix} \mathbf{0} & \mathbf{Y}^\dagger_I \\ \mathbf{X}_I & \mathbf{0} \end{pmatrix} \tag{A4}$$

where $|\mathbf{X}^I\rangle$ and $|\mathbf{X}^I,\mathbf{Y}^I\rangle$ are the transition vectors for the $I$th excited state for TDA and RPA, respectively. Using the expression for the $I$th excited state from eq A3, eq A2 may be evaluated as

$$d^\xi_{0I}(\text{TDA}) = -\sum_{ia\sigma} X^I_{ia\sigma}\langle i;\, \sigma|\nabla_\xi|a;\, \sigma\rangle \tag{A5}$$

$$d^\xi_{0I}(\text{RPA}) = -\sum_{ia\sigma} (X^I_{ia\sigma} - Y^I_{ia\sigma})\langle i;\, \sigma|\nabla_\xi|a;\, \sigma\rangle \tag{A6}$$

Working expressions for the derivative operator in the basis of single particle molecular orbitals may be trivially obtained via direct differentiation.

$$\begin{aligned} \langle p;\, \sigma|\nabla_\xi|q;\, \sigma\rangle &= U^\xi_{pq\sigma} + S^{([\xi])}_{pq\sigma} \\ S^{([\xi])}_{pq\sigma} &= \sum_{\mu\nu} C^*_{\mu p\sigma}\langle\mu|\nu^\xi\rangle C_{\nu q\sigma} \end{aligned} \tag{A7}$$

where $\mathbf{U}^\xi$ is the solution to the coupled-perturbed Kohn−Sham/Hartree−Fock (CPKS/CPHF) equations

$$\begin{aligned} \sum_{jb\sigma'} (\mathbf{A} + \mathbf{B})_{ia\sigma,\text{jb}\sigma'} U^\xi_{jb\sigma'} &= -R_{ia\sigma} \\ R_{ia\sigma} = h^{(\xi)}_{ia\sigma} + v^{H(\xi)}_{ia\sigma} + v^{XC(\xi)}_{ia\sigma} &- \epsilon_i S^{(\xi)}_{ia\sigma} - \frac{1}{2} G^+_{ia\sigma}[S^{(\xi)}_{oo}] \end{aligned} \tag{A8}$$

where the parenthetical superscript denotes differentiation at fixed MOs, $\mathbf{h}$ is the single particle core Hamiltonian, $\{\epsilon_i\}$ is the occupied orbital eigenenergies, $\mathbf{S}^\xi$ is the total derivative of the AO overlap matrix in the MO basis, $v^{\text{H}}$ is the static Hartree term, and $v^{\text{XC}}$ is the static KS-XC potential, which is related to the exchange-correlation kernel, $E_{\text{XC}}$, by

$$v^{\text{XC}}_{ia\sigma} = \sum_{\mu\nu} C^*_{\mu i}\langle\mu|\frac{\partial E_{\text{XC}}}{\partial\rho_\sigma}|\nu\rangle C_{\nu a} \tag{A9}$$

$\mathbf{G}^+$ is the electron-repulsion-integral tensor contracted with the occupied−occupied block of the total derivative of the overlap in the MO basis, $\mathbf{S}^\xi_{oo}$

$$\begin{aligned} G^+_{ia\sigma}[S^{(\xi)}_{oo}] = \sum_{jk\sigma'} (2(ia\sigma|jk\sigma') &- C_x\delta_{\sigma\sigma'}[(ik\sigma|ja\sigma) \\ &+ (ij\sigma|ak\sigma)] + 2(ia\sigma|f^{\sigma\sigma'}_{xc}|jk\sigma'))S^{(\xi)}_{jk} \end{aligned} \tag{A10}$$

where $C_x \in [0,1]$ is the scaling factor for exact HF exchange in hybrid DFT and $f^{\sigma\sigma'}_{\text{XC}}$ is related to the XC kernel by

$$f^{\sigma\sigma'}_{\text{XC}} = \frac{\delta^2 E_{\text{XC}}[\rho(\mathbf{r}, \mathbf{r}')]}{\delta\rho_\sigma(\mathbf{r})\delta\rho_{\sigma'}(\mathbf{r}')} \tag{A11}$$

Inserting eq A7 into eq A5 and eq A6 yields a simple yet inefficient working expressions for the derivative coupling

$$d^\xi_{0I}(\text{TDA}) = -\sum_{ia\sigma} X^I_{ia\sigma} U^\xi_{ia\sigma} - \sum_{ia\sigma} X^I_{ia\sigma} S^{([\xi])}_{ia\sigma} \tag{A12}$$

$$\begin{aligned} d^\xi_{0I}(\text{RPA}) = &-\sum_{ia\sigma} (X^I_{ia\sigma} - Y^I_{ia\sigma}) U^\xi_{ia\sigma} \\ &- \sum_{ia\sigma} (X^I_{ia\sigma} - Y^I_{ia\sigma}) S^{([\xi])}_{ia\sigma} \end{aligned} \tag{A13}$$

One can eliminate the explicit dependence on $\mathbf{U}^\xi$ via a transformation akin to the Sternheimer−Dalgarno interchange theorem[91,92]

$$d^\xi_{0I}(\text{TDA}) = \sum_{ia\sigma} \tilde{Z}^{\text{TDA},I}_{ia\sigma} R^\xi_{ia\sigma} - \sum_{ia\sigma} X^I_{ia\sigma} S^{([\xi])}_{ia\sigma} \tag{A14}$$

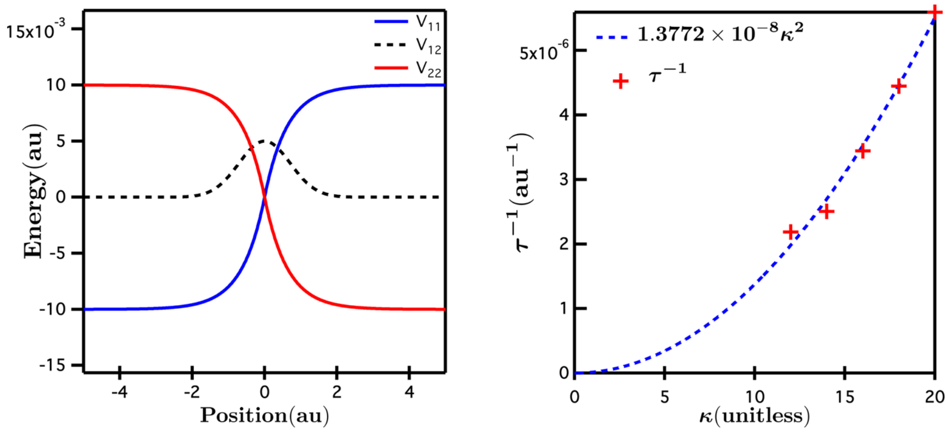

**Figure A1.** Left: Diabatic energy curves and couplings in the region of the surface crossing for the single avoided crossing model problem. Right: Quadratic fit to the surface-hopping transition rates as a function of a coupling biasing factor, $\kappa$, showing consistent proportionality with that expected from the Fermi's golden rule expression.

$$d_{0I}^{\xi}(\mathrm{RPA}) = \sum_{ia\sigma} \tilde{Z}_{ia\sigma}^{\mathrm{RPA},I} R_{ia\sigma}^{\xi} - \sum_{ia\sigma} (X_{ia\sigma}^{I} - Y_{ia\sigma}^{I}) S_{ia\sigma}^{([\xi])} \tag{A15}$$

$$\sum_{jb\sigma'} (\mathbf{A} + \mathbf{B})_{ia\sigma,\mathrm{jb}\sigma'} \tilde{Z}_{jb\sigma'}^{\mathrm{TDA},I} = X_{ia\sigma}^{I} \tag{A16}$$

$$\sum_{jb\sigma'} (\mathbf{A} + \mathbf{B})_{ia\sigma,\mathrm{jb}\sigma'} \tilde{Z}_{jb\sigma'}^{\mathrm{RPA},I} = X_{ia\sigma}^{I} - Y_{ia\sigma}^{I} \tag{A17}$$

While the solution of eq A16 cannot be avoided, the solution of eq A17, as was first recognized by Furche,[47] is known *a priori*,

$$\tilde{Z}_{ia\sigma}^{\mathrm{RPA},I} = \frac{1}{\omega_I}(X_{ia\sigma}^{I} + Y_{ia\sigma}^{I}) \tag{A18}$$

where $\omega_I$ is the excitation energy corresponding to the transition vector $|\mathbf{X}^I,\mathbf{Y}^I\rangle$. Transforming eq A14 and eq A15 into the AO basis, one can obtain an efficient working expression for the derivative coupling closely resembling that of the ground state gradient

$$\begin{aligned} d_{0I}^{\xi}(\mathrm{TDA/RPA}) = {} & \sum_{\mu\nu\sigma} h_{\mu\nu}^{\xi} \tilde{Z}_{\mu\nu\sigma}^{\mathrm{TDA/RPA},I} + \sum_{\mu\nu\sigma} v_{\mu\nu}^{\mathrm{XC}(\xi)} \tilde{Z}_{\mu\nu\sigma}^{\mathrm{TDA/RPA},I} \\ & - \sum_{\mu\nu\sigma} S_{\mu\nu}^{\xi} \tilde{W}_{\mu\nu\sigma}^{\mathrm{TDA/RPA},I} + \sum_{\mu\nu\lambda\delta\sigma\sigma'} (\mu\nu|\lambda\delta)^{\xi} \tilde{\Gamma}_{\mu\nu\sigma,\lambda\delta\sigma'}^{\mathrm{TDA/RPA},I} \\ & + \sum_{\mu\nu\sigma} \tilde{T}_{\mu\nu\sigma}^{\mathrm{TDA/RPA},I} S_{\mu\nu}[\xi] \end{aligned} \tag{A19}$$

where

$$\tilde{T}_{\mu\nu\sigma}^{\mathrm{TDA},I} = \sum_{\mu\nu} C_{\mu i}^{*} X_{ia\sigma}^{I} C_{\nu a};\ \tilde{T}_{\mu\nu\sigma}^{\mathrm{RPA},I} = \sum_{\mu\nu} C_{\mu i}^{*} (X_{ia\sigma}^{I} - Y_{ia\sigma}^{I}) C_{\nu a}$$

$$\tilde{W}_{ia\sigma}^{\mathrm{TDA/RPA},I} = \epsilon_{i\sigma} \tilde{Z}_{ia\sigma}^{\mathrm{TDA/RPA},I};$$

$$\tilde{W}_{ij\sigma}^{\mathrm{TDA/RPA},I} = \frac{1}{1 + \delta_{ij}} G_{ij\sigma}^{+}[\tilde{Z}_{ia\sigma}^{\mathrm{TDA/RPA},I}];$$

$$\tilde{W}_{ab\sigma}^{\mathrm{TDA/RPA},I} = 0$$

$$\begin{aligned} \tilde{\Gamma}_{\mu\nu\sigma,\lambda\delta\sigma'}^{\mathrm{TDA/RPA},I} = {} & \tfrac{1}{2}(2\tilde{Z}_{\mu\nu\sigma}^{\mathrm{TDA/RPA},I} D_{\lambda\delta\sigma'} - C_x \delta_{\sigma\sigma'} \\ & [\tilde{Z}_{\mu\delta\sigma}^{\mathrm{TDA/RPA},I} D_{\lambda\nu\sigma} + \tilde{Z}_{\nu\delta\sigma}^{\mathrm{TDA/RPA},I} D_{\lambda\mu\sigma}]) \end{aligned}$$

where $\mathbf{D}$ is the ground state KS/HF density.

## APPENDIX 2: META-SURFACE-HOPPING METHOD VALIDATED ON ONE-DIMENSIONAL SINGLE AVOIDED CROSSING PROBLEM

The robustness of the MSH method relies on the surface hopping and perturbative-derived transition rates being affected proportionately by an artificial magnification of the coupling strength between states. As was derived in the main text (eq 22), the Fermi's golden rule transition probability depends quadratically on the biasing strength parameter, $\kappa$. However, the coupling strength only explicitly enters into the FSSH transition probability expression (eq 10) linearly. For these two approaches to yield consistent behavior upon scaling of the coupling, the effect of the heightened coupling on the composition of the evolving electronic wavepacket must account for the "missing power" of the scaling factor in the FSSH transition probability expression. From eq 8, it is clear that the evolution of the density matrix elements that enter into the FSSH probability expression depends nonlinearly on the scaling factor, $\kappa$, so unlike the TDPT approach, no simple closed form relationship can be derived between $\kappa$ and the FSSH transition probability. Instead, numerical evidence that the inclusion of the magnified coupling in the electronic propagation effectively accounts for the apparent discrepancy between the surface hopping, and TDPT transition probabilities must suffice.

To numerically probe the relationship between the FSSH relaxation rates and a constant factor scaling the coupling strength between the quantum states of a system, the MSH method was applied to a single avoided crossing model problem defined by the following Hamiltonian in the diabatic representation:[70]

$$\begin{aligned} V_{11}(R) &= A[1 - \mathrm{Exp}[-BR]],\ R \geq 0 \\ V_{11}(R) &= -A[1 - \mathrm{Exp}[-BR]],\ R \leq 0 \\ V_{22}(R) &= -V_{11}(R) \\ V_{12}(R) &= V_{21}(R) = C\mathrm{Exp}[-DR^2] \end{aligned} \tag{B1}$$

Surface hopping trajectories were evaluated directly in the diabatic basis. For the MSH biasing procedure, the diabatic couplings (rather than the analogous derivative couplings between adiabats which vanish in the diabatic representation) were uniformly scaled by $\kappa$. For the purposes of isolating the effect of the scaled couplings on the surface hopping rates, only relaxation events prior to the diabatic surface crossing (i.e., those induced by surface hops) are considered in the transition rate statistics. In this way, a finite maximum lifetime was effectively imposed on the excited state, leading to a nonzero rate for the $\kappa \to 0$ limit that was accounted for prior to the collection of transition statistics.

A total of 10,000 independent trajectories were computed for different values of $\kappa$ to determine the mean (surface hopping) lifetimes for each biasing strength. All trajectories were initialized in the upper diabatic state and share common classical initial conditions and model parameters ($R(0) = -2$, $\dot{R}(0) = 0$, $A = 0.01$, $B = 1.6$, $C = 0.005$, and $D = 1.0$). The quadratic dependence of the FSSH transition rate on the biasing strength (Figure A1) observed for the model problem shows with a high degree of statistical certainty that average hopping probabilities are consistent with the TDPT result for certain ranges of biasing strengths and that hybrid dynamical/perturbative methods are a promising direction for investigating slow transitions via biased time-domain simulations.

## ■ AUTHOR INFORMATION

### Corresponding Author

*E-mail: xsli@uw.edu.

### Notes

The authors declare no competing financial interest.

## ■ ACKNOWLEDGMENTS

This work is supported by the U.S. National Science Foundation (CHE-1265945, CHE-1464497). The University of Washington Student Technology Fund provided computational resources to enable this work. D.B.L. is grateful for the University of Washington Clean Energy Institute Fellowship.

## ■ REFERENCES

(1) Marx, D.; Hutter, J. *Ab Initio Molecular Dynamics: Basic Theory and Advanced Methods*; Cambridge University Press, 2009.
(2) Lorenz, C.; Doltsinis, N. In *Handbook of Computational Chemistry*; Leszczynski, J., Ed.; Springer: The Netherlands, 2014; pp 195−238.
(3) Frenkel, D.; Smit, B. *Understanding Molecular Simulation: From Algorithms to Applications*; Computational Science Series; Elsevier Science, 2001.
(4) Lingerfelt, D. B.; Fischer, S. A.; May, J. W.; Li, X. *J. Phys. Chem. C* **2014**, *118*, 3266−3273.
(5) Heller, E. J. *Acc. Chem. Res.* **1981**, *14*, 368−375.
(6) Barbatti, M.; Aquino, A. J. A.; Lischka, H. *Phys. Chem. Chem. Phys.* **2010**, *12*, 4959−4967.
(7) Petit, A. S.; Subotnik, J. E. *J. Chem. Phys.* **2014**, *141*, 154108.
(8) Mikosch, J.; Trippel, S.; Eichhorn, C.; Otto, R.; Lourderaj, U.; Zhang, J. X.; Hase, W. L.; Weidemüller, M.; Wester, R. *Science* **2008**, *319*, 183−186.
(9) Marrink, S. J.; Mark, A. E. *J. Am. Chem. Soc.* **2003**, *125*, 11144−11145.
(10) Xie, W.; Bai, S.; Zhu, L.; Shi, Q. *J. Phys. Chem. A* **2013**, *117*, 6196−6204.
(11) Hammes-Schiffer, S.; Tully, J. C. *J. Chem. Phys.* **1994**, *101*, 4657−4667.
(12) Kosloff, R. *J. Phys. Chem.* **1988**, *92*, 2087−2100.
(13) Light, J. C.; Carrington, T. *Advances in Chemical Physics*; John Wiley and Sons, Inc., 2007; pp 263−310.
(14) Meyer, H.-D.; Manthe, U.; Cederbaum, L. *Chem. Phys. Lett.* **1990**, *165*, 73−78.
(15) Tully, J. *Faraday Discuss.* **1998**, *110*, 407−419.
(16) Kapral, R.; Ciccotti, G. *J. Chem. Phys.* **1999**, *110*, 8919−8929.
(17) Deumens, E.; Diz, A.; Longo, R.; Öhrn, Y. *Rev. Mod. Phys.* **1994**, *66*, 917−983.
(18) Bastida, A.; Cruz, C.; Zúñiga, J.; Requena, A.; Miguel, B. *Chem. Phys. Lett.* **2006**, *417*, 53−57.
(19) Born, M.; Oppenheimer, R. *Ann. Phys.* **1927**, *389*, 457−484.
(20) Kutzelnigg, W. *Mol. Phys.* **2007**, *105*, 2627−2647.
(21) Massey, H. S. W. *Rep. Prog. Phys.* **1949**, *12*, 248.
(22) Morrissey, B. W. *J. Chem. Educ.* **1975**, *52*, 296−298.
(23) Parandekar, P. V.; Tully, J. C. *J. Chem. Phys.* **2005**, *122*, 094102.
(24) Parandekar, P. V.; Tully, J. C. *J. Chem. Theory Comput.* **2006**, *2*, 229−235.
(25) Horsfield, A. P.; Bowler, D.; Fisher, A.; Todorov, T. N.; Sánchez, C. G. *J. Phys.: Condens. Matter* **2004**, *16*, 8251.
(26) Kelly, A.; Brackbill, N.; Markland, T. E. *J. Chem. Phys.* **2015**, *142*, 094110.
(27) Martinez, T. J.; Ben-Nun, M.; Levine, R. D. *J. Phys. Chem.* **1996**, *100*, 7884−7895.
(28) Craig, I. R.; Manolopoulos, D. E. *J. Chem. Phys.* **2004**, *121*, 3368−3373.
(29) Richardson, J. O.; Thoss, M. *J. Chem. Phys.* **2013**, *139*, 031102.
(30) Cao, J.; Voth, G. A. *J. Chem. Phys.* **1994**, *100*, 5106−5117.
(31) Hack, M. D.; Wensmann, A. M.; Truhlar, D. G.; Ben-Nun, M.; Martinez, T. J. *J. Chem. Phys.* **2001**, *115*, 1172−1186.
(32) Worth, G. A.; Hunt, P.; Robb, M. A. *J. Phys. Chem. A* **2003**, *107*, 621−631.
(33) Barbatti, M. *WIRES Comput. Mol. Sci.* **2011**, *1*, 620−633.
(34) Bjerre, A.; Nikitin, E. *Chem. Phys. Lett.* **1967**, *1*, 179−181.
(35) Tully, J. C.; Preston, R. K. *J. Chem. Phys.* **1971**, *55*, 562−572.
(36) Craig, C. F.; Duncan, W. R.; Prezhdo, O. V. *Phys. Rev. Lett.* **2005**, *95*, 163001.
(37) Tapavicza, E.; Tavernelli, I.; Rothlisberger, U. *Phys. Rev. Lett.* **2007**, *98*, 023001.
(38) Plasser, F.; Crespo-Otero, R.; Pederzoli, M.; Pittner, J.; Lischka, H.; Barbatti, M. *J. Chem. Theory Comput.* **2014**, *10*, 1395−1405.
(39) Du, L.; Lan, Z. *J. Chem. Theory Comput.* **2015**, *11*, 1360−1374.
(40) Akimov, A. V.; Prezhdo, O. V. *J. Chem. Theory Comput.* **2013**, *9*, 4959−4972.
(41) Barbatti, M.; Ruckenbauer, M.; Plasser, F.; Pittner, J.; Granucci, G.; Persico, M.; Lischka, H. *WIRES Comput. Mol. Sci.* **2014**, *4*, 26−33.
(42) Richter, M.; Marquetand, P.; Gonzalez-Vazquez, J.; Sola, I.; Gonzalez, L. *J. Chem. Theory Comput.* **2011**, *7*, 1253−1258.
(43) Zheng, J.; Li, Z.-H.; Jasper, A. W.; Bonhommeau, D. A.; Valero, R.; Meana-Pañeda, R.; Truhlar, D. G. ANT, version 2015. http://comp.chem.umn.edu/ant (accessed February 2016).
(44) Alguire, E. C.; Ou, Q.; Subotnik, J. E. *J. Phys. Chem. B* **2015**, *119*, 7140−7149.
(45) Ou, Q.; Alguire, E. C.; Subotnik, J. E. *J. Phys. Chem. B* **2015**, *119*, 7150−7161.
(46) Fatehi, S.; Alguire, E.; Shao, Y.; Subotnik, J. E. *J. Chem. Phys.* **2011**, *135*, 234105.
(47) Send, R.; Furche, F. *J. Chem. Phys.* **2010**, *132*, 044107.
(48) Zhang, X.; Herbert, J. M. *J. Chem. Phys.* **2015**, *142*, 064109.
(49) Li, Z.; Suo, B.; Liu, W. *J. Chem. Phys.* **2014**, *141*, 244105.
(50) Runge, E.; Gross, E. K. U. *Phys. Rev. Lett.* **1984**, *52*, 997−1000.
(51) Xu, B. X.; Rajagopal, A. K. *Phys. Rev. A: At., Mol., Opt. Phys.* **1985**, *31*, 2682.
(52) Dhara, A. K.; Ghosh, S. K. *Phys. Rev. A: At., Mol., Opt. Phys.* **1987**, *35*, 442.
(53) Chen, G. H.; Mukamel, S. *J. Chem. Phys.* **1995**, *103*, 9355.
(54) Casida, M. E. *Recent Developments and Applications in Density Functional Theory*; Elsevier: Amsterdam, 1996.
(55) Yabana, K.; Bertsch, G. F. *Phys. Rev. B: Condens. Matter Mater. Phys.* **1996**, *54*, 4484.
(56) Marques, M. A. L.; Gross, E. K. U. *Annu. Rev. Phys. Chem.* **2004**, *55*, 427.
(57) Burke, K.; Werschnik, J.; Gross, E. K. U. *J. Chem. Phys.* **2005**, *123*, 062206.
(58) Kulander, K. C. *Phys. Rev. A: At., Mol., Opt. Phys.* **1987**, *36*, 2726.
(59) Kulander, K. C. *Phys. Rev. A: At., Mol., Opt. Phys.* **1987**, *35*, 445.

(60) Field, M. J. *J. Chem. Phys.* **1992**, *96*, 4583.

(61) Liang, W.; Fischer, S. A.; Frisch, M. J.; Li, X. *J. Chem. Theory Comput.* **2011**, *7*, 3540−3547.

(62) Handy, N. C.; Lee, A. M. *Chem. Phys. Lett.* **1996**, *252*, 425−430.

(63) Ben-Nun, M.; Levine, R. *Chem. Phys.* **1995**, *201*, 163−187.

(64) Feng, W.; Xu, L.; Li, X.-Q.; Fang, W.; Yan, Y. *AIP Adv.* **2014**, *4*, 077131.

(65) Martens, C. C.; Fang, J.-Y. *J. Chem. Phys.* **1997**, *106*, 4918−4930.

(66) Burant, J. C.; Tully, J. C. *J. Chem. Phys.* **2000**, *112*, 6097−6103.

(67) Cheng, S. C.; Zhu, C.; Liang, K. K.; Lin, S. H.; Truhlar, D. G. *J. Chem. Phys.* **2008**, *129*, 024112.

(68) Shenvi, N.; Subotnik, J. E.; Yang, W. *J. Chem. Phys.* **2011**, *134*, 144102.

(69) Krishna, V. *J. Chem. Phys.* **2007**, *126*, 134107.

(70) Tully, J. C. *J. Chem. Phys.* **1990**, *93*, 1061−1071.

(71) Jasper, A. W.; Stechmann, S. N.; Truhlar, D. G. *J. Chem. Phys.* **2002**, *116*, 5424−5431.

(72) Frisch, M. J.; Trucks, G. W.; Schlegel, H. B.; Scuseria, G. E.; Robb, M. A.; Cheeseman, J. R.; Scalmani, G.; Barone, V.; Mennucci, B.; Petersson, G. A.; Nakatsuji, H.; Caricato, M.; Li, X.; Hratchian, H. P.; Izmaylov, A. F.; Bloino, J.; Zheng, G.; Sonnenberg, J. L.; Liang, W.; Hada, M.; Ehara, M.; Toyota, K.; Fukuda, R.; Hasegawa, J.; Ishida, M.; Nakajima, T.; Honda, Y.; Kitao, O.; Nakai, H.; Vreven, T.; J. A. Montgomery, J.; Peralta, J. E.; Ogliaro, F.; Bearpark, M.; Heyd, J. J.; Brothers, E.; Kudin, K. N.; Staroverov, V. N.; Keith, T.; Kobayashi, R.; Normand, J.; Raghavachari, K.; Rendell, A.; Burant, J. C.; Iyengar, S. S.; Tomasi, J.; Cossi, M.; Rega, N.; Millam, J. M.; Klene, M.; Knox, J. E.; Cross, J. B.; Bakken, V.; Adamo, C.; Jaramillo, J.; Gomperts, R.; Stratmann, R. E.; Yazyev, O.; Austin, A. J.; Cammi, R.; Pomelli, C.; Ochterski, J. W.; Martin, R. L.; Morokuma, K.; Zakrzewski, V. G.; Voth, G. A.; Salvador, P.; Dannenberg, J. J.; Dapprich, S.; Parandekar, P. V.; Mayhall, N. J.; Daniels, A. D.; Farkas, O.; Foresman, J. B.; Ortiz, J. V.; Cioslowski, J.; Fox, D. J. Gaussian Development Version, Revision H.21. Gaussian, Inc., Wallingford CT, 2012.

(73) Millam, J. M.; Bakken, V.; Chen, W.; Hase, W. L.; Schlegel, H. B. *J. Chem. Phys.* **1999**, *111*, 3800−3805.

(74) Li, X.; Millam, J. M.; Schlegel, H. B. *J. Chem. Phys.* **2001**, *114*, 8897−8904.

(75) Li, X.; Smith, S. M.; Markevitch, A. N.; Romanov, D. A.; Levis, R. J.; Schlegel, H. B. *Phys. Chem. Chem. Phys.* **2005**, *7*, 233−239.

(76) Li, X.; Tully, J. C.; Schlegel, H. B.; Frisch, M. J. *J. Chem. Phys.* **2005**, *123*, 084106.

(77) Malhado, J. P.; Bearpark, M. J.; Hynes, J. T. *Front. Chem.* **2014**, *2*, 97.

(78) Fernandez-Alberti, S.; Roitberg, A. E.; Nelson, T.; Tretiak, S. *J. Chem. Phys.* **2012**, *137*, 014512.

(79) Wang, L.; Prezhdo, O. V. *J. Phys. Chem. Lett.* **2014**, *5*, 713−719.

(80) Laio, A.; Parrinello, M. *Proc. Natl. Acad. Sci. U. S. A.* **2002**, *99*, 12562−12566.

(81) Laio, A.; Gervasio, F. L. *Rep. Prog. Phys.* **2008**, *71*, 126601.

(82) Fischer, S. A.; Chapman, C. T.; Li, X. *J. Chem. Phys.* **2011**, *135*, 144102.

(83) Hammes-Schiffer, S.; Tully, J. C. *J. Chem. Phys.* **1995**, *103*, 8528−8537.

(84) Nangia, S.; Jasper, A. W.; Miller, T. F.; Truhlar, D. G. *J. Chem. Phys.* **2004**, *120*, 3586−3597.

(85) Cohen-Tannoudji, C.; Diu, B.; Laloe, F. *Quantum Mechanics*; Wiley, 1991; Vl. 1, pp 1283−1303.

(86) Schatz, G.; Ratner, M. *Quantum Mechanics in Chemistry*; Dover Publications, 2012; pp 70−74.

(87) Sauer, S. *Molecular Electromagnetism: A Computational Chemistry Approach*; Oxford University Press: Oxford, 2011; pp 30−66.

(88) Peslherbe, G. H.; Wang, H.; Hase, W. L. *Advances in Chemical Physics*; John Wiley and Sons, Inc., 2007; pp 171−201.

(89) Hase, W. L.; Duchovic, R.J.; Komornicki, A.; Lim, K. F.; Lu, D.-H.; Peslherbe, G. H.; Swamy, K. N.; Linde, S. R. V.; Varandas, A.; Wang, H.; Wolf, R. J. *Quant. Chem. Prog. Exch.* **1996**, *16*, 671.

(90) Kilina, S. V.; Kilin, D. S.; Prezhdo, V. V.; Prezhdo, O. V. *J. Phys. Chem. C* **2011**, *115*, 21641−21651.

(91) Dalgarno, A.; Stewart, A. L. *Proc. R. Soc. London, Ser. A* **1958**, *247*, 245−259.

(92) Sternheimer, R. M.; Foley, H. M. *Phys. Rev.* **1953**, *92*, 1460−1468.

DOI: 10.1021/acs.jctc.5b00697
*J. Chem. Theory Comput.* 2016, 12, 935−945